

A High Resolution Mosaic of Molecular Gas in Stephan's Quintet

Glen R. Petitpas

Smithsonian Astrophysical Observatory

645 N. A'ohoku Place, Hilo, HI, USA 96720

`gpetitpas@cfa.harvard.edu`

and

Christopher L. Taylor

California State University, Sacramento

6000 J Street, Sacramento, CA, USA 95819

`ctaylor@csus.edu`

ABSTRACT

We present high resolution $^{12}\text{CO } J=1-0$ observations of the molecular gas in the Hickson Compact Group Stephan's Quintet (HCG92). Our observations consist of multiple pointing and mosaics covering all the regions where CO and star formation has been detected. Within the $100''$ field of view centered on the eastern-most tidal tail, we detect three clumps of emission that may be partially resolved at our resolution of $8''$; two of these are new detections not previously seen in ISM studies of this region. Two of these clumps lie in the optical tidal tail, while the third lies to the southeast and is coincident with a large H I feature, but does not correspond to any features at other wavelengths. We also tentatively detect CO emission from the star forming regions in the "Old Tail" corresponding to recent star formation activity detected in recent UV and H α observations. Observations of the rest of the compact group do not show detections even though strong emission was detected with single dish telescopes, which suggests the CO emission originates from a diffuse molecular gas cloud or from more at least three separate clumps with separations of greater than around 3 kpc.

Subject headings: Galaxies: interactions – galaxies:ISM – galaxies:clusters:individual (HCG92, Stephan's Quintet) – intergalactic medium

1. Introduction

The parallel studies of dwarf galaxies and the outer regions of spiral galaxies have come together as awareness has grown of the apparent formation of new dwarf galaxies in the tidal arms of merging and interacting systems. These galaxies are referred to as “Tidal Dwarf Galaxies” (hereafter TDGs). The concept of material from interacting galaxies being thrown out of interacting galaxies and forming new galaxies is old (Zwicky 1956; Schweizer 1978). This idea has been revived since the early 1990’s by Mirabel and collaborators, who found patches of enhanced optical emission along the tidal tails of interacting systems (e.g., Mirabel, Lutz, & Maza 1991) and subsequently found that these patches correlate closely with local enhancements in the column density of H I (e.g., Duc & Mirabel 1994; Duc et al. 1997).

Studies of the physical properties of TDGs show that they are very similar in gas mass and size to typical gas rich dwarfs such as dwarf irregulars (dIs) and blue compact dwarfs (BCDs; Duc et al. 2001; Braine et al. 2001). One difference is that the metallicities of TDGs tend to cluster at the metal rich end of the range found for the general dI and BCD populations. In fact, the metallicities of TDGs are consistent with their ISMs being composed of gas from the outer disks of spiral galaxies.

Some TDGs and candidate TDGs show signs of recent star formation, such as blue colors and H α emission (e.g., Duc & Mirabel 1994; Iglesias-Paramo & Vilchez 2001), which implies the presence of molecular gas. Because TDGs are more metal rich than typical dIs and BCDs, they may be brighter in CO emission than dIs and BCDs (Taylor, Kobulnicky, & Skillman 1998). Indeed, several TDGs have been detected in CO emission (Braine et al. 2001), although not yet in sufficient numbers to say for certain that they are easier to detect than dIs and BCDs in CO.

Several issues surrounding TDGs remain unresolved, including whether or not they are truly self-gravitating, newly formed galaxies, whether the CO-to-H $_2$ conversion factor is higher than in dIs and BCDs, and whether their molecular gas is formed *in situ* from atomic gas, or is already in molecular form when expelled from the parent merging system. To shed some light on these issues, we have made a wide-field mosaic image in the $^{12}\text{CO } J=1-0$ line of the Hickson Compact Group 92, also known as Stephan’s Quintet.

Stephan’s Quintet is a group of five galaxies (only three are interacting) contained in a relatively small region of space. The result of living within such close proximity is that there are a larger number of interactions between neighboring galaxies than is found in larger clusters of galaxies, where the relative distances and velocities are larger. It is believed that an intruder galaxy (NGC 7320c) passed through the center of this system, depositing a

reservoir of molecular gas that was later disrupted by the passage of NGC 7318b to trigger star formation in the intergalactic medium (e.g., Charlton et al. 2004).

This system is also the host of a recently discovered extragalactic starburst (Xu, Sulentic, & Tuffs 1999), and has been mapped in CO at low spatial resolution over most of its spatial extent (Lisenfeld et al. 2002), or at high spatial resolution in a single field (Gao & Xu 2000; Lisenfeld et al. 2004). Iglesias-Paramo & Vilchez (2001) identified seven extragalactic H α emitting regions in HCG 92 which may be TDGs. Ours is the first wide-field, high resolution survey of CO emission in the compact group, and in 6 of these seven TDG candidates.

2. Observations and Reduction

2.1. BIMA Observations of $^{12}\text{CO } J=1-0$

We have observed three regions of the intergalactic medium in the interacting system HCG 92 corresponding to the regions observed in the tidal dwarf galaxy survey of Lisenfeld et al. 2002 (their regions A, B, and C). In addition, we have performed a 7-field mosaic the “Arc-N” region to the north of the tidal tail (see Figure 1; Williams, Yun, & Verdes-Montenegro 2002). The observations were taken over a period of 2002 May 11 - 2002 Oct 19 using the 10 element Berkeley-Illinois-Maryland Association (BIMA) millimeter interferometer at Hat Creek California (Welch et al. 1996). Our observations include 4 D array and 2 C array tracks on each region mentioned above. We observed at the $^{12}\text{CO } J=1-0$ spectral line (115.27 GHz) Doppler shifted to a V_{LSR} given in column 4 Table 1 (optical definition) with a spectral raw resolution of 1.56 MHz, (4.06 km s $^{-1}$) with a total bandwidth of 386 GHz (960 km s $^{-1}$). When bright emission was detected at region B, we followed up with more 2 C array and 2 more D array tracks to increase signal to noise. The combined data set includes baselines that range from 7 m to 88 m. The final synthesized beam approximately 8'' for each of the regions.

In addition to the the C- and D-array tracks for Region B, we obtained two B-array tracks at a resolution of 2''. No emission was detected in these data alone, and their inclusion into the combined maps introduced artifacts and generally degraded the image quality. Thus, the B-array data was not included in the final maps shown here.

The CO emission for regions A, B, and C were believed to be relatively centrally concentrated (Lisenfeld et al. 2002), so we observed these regions with single pointings so as to not to use precious integration time slewing. For the Arc-N region, we had no expectations of how extended any CO emission may be, but there were reports of extended star formation to the north of the tidal tail. We opted for the mosaic in order to increase the area covered

by our map. The primary beam of a single point observation with the BIMA array at 115 GHz is $100''$, but with the 7-field mosaic, we are capable of covering a area with a much flatter sensitivity in the inner $100''$, and an effective primary beam of around $180''$. Details of the mosaic procedure are given in Helfer et al. (2003).

Observing parameters for each pointing center are given in Table 1. The first column is the label for each region we observed. The second and third columns are the right ascension and declination for the pointing centers of our observations. The fourth column is the velocity to which we tuned, and the fifth column is the number of pointings observed with these settings. The sixth, seventh and eighth columns are the effective field of view, synthesized beam (resolution) and r.m.s. noise for each of the regions observed. Note that all fields in this study are single pointings except for the “Arc-N” observations, which were done with a 7-field mosaic, and thus have a higher noise level due to the overhead caused by slewing during the track.

The data were calibrated and reduced using the MIRIAD data reduction package (Sault, Teuben, & Wright 1995). Instrumental and atmospheric phase variations were measured by observing the quasar 2203+317 every 25 minutes. Amplitude calibration was performed using various planets as primary flux calibrators. The data were weighted using the robust weighting parameter of 0.5. The final channel maps have an r.m.s. noise of $\sim 2 - 4 \times 10^{-2}$ Jy $\text{bm}^{-1} \text{km s}^{-1}$.

3. Morphology

3.1. Region A: The Intragroup Starburst

Previous observations of this region show CO emission that originates from the center of the intragroup starburst (IGS). Unfortunately, observations are complicated by the existence of two emission regions separated in velocity space: one at around 6000 km s^{-1} , and the other at around 6700 km s^{-1} . Despite the weakness of the CO emission at 6700 km s^{-1} observed by Gao & Xu (2000), the reality of their detection is supported by the fact that it peaks near the center of the starburst detected in the mid-IR and H- α maps of Xu, Sulentic, & Tuffs (1999) and is at the same velocity of one of the H I components (Williams, Yun, & Verdes-Montenegro 2002). The lower velocity CO emission was detected with the IRAM 30m by Lisenfeld et al. (2002) and is reported to be more than twice as strong as the higher velocity component. There is also star formation activity observed at the lower velocity component as traced by the H α observations of Xu, Sulentic, & Tuffs (1999) (although it appears at around 5700 km s^{-1} , not 6000 km s^{-1} like the CO detections).

Because the BIMA receivers cannot cover both emission regions with the desired velocity resolution, we decided to observe the brighter (previously unmapped at high resolution) low velocity component. Despite reaching an r.m.s. noise of 21 mJy bm^{-1} in the map (at 5 km s^{-1} resolution) we do not detect CO emission from this region. This is somewhat surprising since the H I column density and single dish $^{12}\text{CO } J=1-0$ fluxes of CO emission in Region A are actually approximately equal or greater in intensity than the detections in Region B (Williams, Yun, & Verdes-Montenegro 2002; Lisenfeld et al. 2002), which we do detect. Thus the gas must have a more even distribution rendering our interferometric observations less sensitive to this more diffuse emission. We note that with our tuning setup, we are unable to confirm the existence of the IGM emission observed by Gao & Xu (2000) since it lies outside our velocity range at a higher velocity.

The IRAM 30m detection has a peak of $\sim 17 \text{ mK}$ (T_{MB}) in a 10 km s^{-1} channel which corresponds to a 75 mJy peak. Thus we would have expected to see >3 sigma detection if the flux detected in the IRAM beam were a point source. Conversely, if the flux detected by IRAM were uniformly distributed across the $21''$ beam, we would expect a flux of 8 mJy , which we would not have detected in our BIMA map. If the flux detected by the single dish observations were originating from two unresolved clumps, we would still predicted 1.5 sigma detections from these clouds. We can therefore conclude that the molecular gas in the IGS is not made up of one small clump, but either a more diffuse distribution, or at least 3 clumps separated by more than about $8''$ (3.4 kpc at 88 Mpc).

Figure 2 (upper left panel) shows the moment 0 map overlain with the 2,3,4 sigma contours. The 3 sigma contours are simply the result of spikes in the spectra that happen to lie within the velocity range over which this moment map was made and do not correspond to significant real emission. There is a clear lack of CO emission at the peak of the H I maps (overlaid with gray contours). One possible explanation for this could lie in the existence of two different velocity components at this region. We were only capable of covering one within our tuning set up and choose the brightest of the two, as seen in the single dish CO maps of Lisenfeld et al. (2002). It is possible that the component that is brighter in the single dish maps (at 6000 km s^{-1}) contains more diffuse emission and perhaps the component at 6700 km s^{-1} contains more dense clumps which were diluted in the single dish maps. Follow up observations of this region tuned to the 6700 km s^{-1} component would be useful in characterizing this region in more detail.

3.2. Region B: The Tidal Tail

Previous studies of this region show the H I peaks near the intersection of the southern-most arc of the optical tidal tail with the Arc-N portion of the H I distribution. Previous single dish $^{12}\text{CO } J=1-0$ observations show strong emission from the optical tail region (Lisenfeld et al. 2002). Follow-up Plateau de Bure interferometric observations (Lisenfeld et al. 2004) show this emission originates from the star forming region detected by Iglesias-Paramo & Vilchez (2001) and lies on the dust lanes seen in the HST images of Gallagher et al. (2001). Lisenfeld et al. (2004) detect two emission regions: one at the star forming dust lane (SQ B) and one at the tip of the optical tidal tail (SQ tip). We do not detect CO at the tip of the tidal tail, but it is a weak, marginal detection in the more sensitive data of (Lisenfeld et al. 2004), so it is not unexpected that we do not recover it with our less sensitive BIMA data.

With our lower sensitivity, but larger field of view observations, we detect three clumps of CO emission in the eastern-most tidal tail of HCG 92 (Region B). Two of the clumps (SQB and SQB NW) lie directly on the tidal tail and correspond well with dust lanes observed in the HST images from Gallagher et al. (2001). Figures 3 and 4 show these clumps overlaid on HST and DSS images, and the correspondence with the dust lanes is obvious for the clumps that lie on the optical tail. We note that the earlier CO observation of HCG 92 (in particular NGC 7318, Yun et al. 1997; Gao & Xu 2000) show the CO emission in the parent galaxy also corresponds well with the dusty regions visible in the HST images (Gallagher et al. 2001, Figure 3). The correspondence of these regions of CO emission with the dust lanes is not surprising. It is suspected that the same high density environment that provide shielding against dissociation of dust molecules also provides conditions conducive to the formation of molecules (e.g. Alves, Lada, & Lada 1999, and references therein).

The detection of SQB NW is new with our observations – the Plateau de Bure interferometer maps of Lisenfeld et al. (2004) do not show it. Our detection of SQB NW falls outside the primary beam of the PdB interferometer, thus the observations of Lisenfeld et al. (2004) were not sensitive to this emission region. The same authors in Lisenfeld et al. (2002) did not observe the location of SQB NW in their IRAM 30m mapping of HCG 92. SQB NW does not have any corresponding H I emission in the VLA map by Williams, Yun, & Verdes-Montenegro (2002).

In addition to the two clumps in the tail, we detect a clump of molecular gas to the south-east of the tail (SQB SE). This emission region does not correspond with any previous observed star forming regions or evident dust obscuration. Also, it seem to be at a slightly different velocity than the other two regions in the tail (see Table 2). Figure 3 shows the H I contours (Williams, Yun, & Verdes-Montenegro 2002) on the CO contours. While the CO

emission at SQB SE does not correspond with any features visible, it does lie within the H I cloud designated as “Arc-N” by Williams, Yun, & Verdes-Montenegro (2002). None of the peaks in the CO emission we detect correspond with the H I peak of the Arc-N region. The two eastern-most peaks seem to straddle the H I peak, while the western CO peak does not correspond with any significant H I emission. Lisenfeld et al. (2002) pointed out that SQB does not lie at the peak of the H I emission, but rather at the location of a steep gradient in H I column density, and they suggest that perhaps compression of the atomic gas at this location leads to formation of molecular gas. We further point out that both the SQ tip detection by (Lisenfeld et al. 2004) and our new detection of SQB SE similarly lie on the edges of the peak in H I column density. The density gradient at the location of SQB is larger than for SQ tip and SQB SE, which may explain why there is more CO emission at these locations.

Figure 5 shows the individual CO emission lines (solid) with the H I spectra overlaid with the dashed line in the “New Tail” region.. The CO lines tend to lie within the envelope of the H I line, but skewed slightly toward the higher velocity tail. This was not noted by Lisenfeld et al. (2004), who find good agreement of the centroid velocities of the H I and CO in their higher resolution maps. Comparing our spectra with those of Lisenfeld et al. (2004) we find that our maps seem to be missing some emission between the velocity range of 6576 - 6600 km s⁻¹. This is somewhat surprising since our data are lower resolution and should be more sensitive to more extended structure. It is likely that our observations are less sensitive to this emission due to the larger collecting area of the IRAM Plateau de Bure interferometer compared to the BIMA array. Since the source is barely resolved for both telescopes, spatial filtering is not as much of a loss of signal as the difference in collecting area.

The two extreme southern-most clumps lie in the middle of the “Old Tail.” This feature appears as a faint optical structure that passes behind the foreground galaxy NGC 7320 and has an H I counterpart (Williams, Yun, & Verdes-Montenegro 2002). The origin of this tail is uncertain, and has recently been ascribed to an old passage of NGC 7320c that pulled the tail out of NGC 7318A (Williams, Yun, & Verdes-Montenegro 2002; Sulentic et al. 2001). The same authors also ascribe the more prominent tidal tail (which encompasses the CO detections SQB, SQ tip and SQ NW) to a more recent passage of NGC 7320c that pulled a tail out of NGC 7319.

The two southern-most clumps OT1 and OT2 lie just outside the edge of the BIMA primary beam. In an interferometer map, the sensitivity of the telescope declines in an approximately Gaussian fashion from the center to the edge. Normally objects appearing at the edge of the primary beam (where the sensitivity has dropped to 50% that of the map center) would not be considered seriously. However, both OT1 and OT2 show significant

flux across 4 and 5 channels respectively, even taking into account the reduced sensitivity (Figure 6). Unfortunately the ongoing construction of the CARMA interferometer from the antennae of BIMA and OVRO has made it impossible to obtain new observations centered on the locations of OT1 and OT2.

If OT1 and OT2 are real, they might be molecular gas associated with the “Old Tail”, which they overlap spatially. Sulentic et al. (2001) use various estimators to derive an age of this tail between 6 and 12×10^8 yr, compared to 2 to 4×10^8 yr for the more visually prominent younger tail. If OT1 and OT2 are “Old Tail” clouds, they may have existed in intergalactic space for $\sim 10^8$ yr. Alternately they may have formed more recently, triggered by the interaction of NGC 7320c with the gas in the “Old Tail” during its second passage through the group.

OT1 and OT2 also overlap spatially with a region of far UV emission detected by *GALEX* which yielded an age of $\sim 3 \times 10^8$ yr for the stellar populations and a current star formation rate of $0.060 \pm 0.013 M_{\odot}\text{yr}^{-1}$ (Xu et al. 2005).

In the Old Tail region, the velocity offset between the CO and H I emission is similar to the offset seen in the “New Tail” (see Figure 6 and Table 6). The offset appears to be slightly larger in the “Old Tail” region compared to the “New Tail” emission since in these regions, we do not see any high velocity tail and do not have the signal to noise to detect any such tail in our lines.

3.3. SQ C: Star Forming Tidal Dwarf Galaxies?

Region C in Figure 3 lies to the west of Region B, and is the site of a number of candidate TDGs listed by (Mendes de Oliveira et al. 2001), who isolated them based upon $H\alpha$ emission. (Lisenfeld et al. 2002) did not detect CO emission from any of these candidates in IRAM 30m observations targeted at them and at a few nearby local H I maxima. Our single BIMA pointing covers the entire region and places an upper limit of $25 \text{ mJy } \text{bm}^{-1}$. Although there are indeed a number of star clusters in this area coincident with the $H\alpha$ emitting regions (see the analysis of the data of Gallagher et al. (2001) by Lisenfeld et al. (2002)), in the absence of any kinematically distinct component of ISM, no strong case can be made for the presence of TDGs in the western side of HCG 92.

3.4. Arc-N: Star Formation Without an Optical Tail?

The Arc-N region (Williams, Yun, & Verdes-Montenegro 2002) is an H I rich gaseous tail that is likely the result of the gas in the parent galaxies (NGC 7319, NGC 7318a,b) being stripped out by the rapid passage of NGC 7320c through the system. Recent GALEX images show UV emission originating from various regions within the Arc-N area (Xu et al. 2005). This the strength of this emission is indicative of star formation rates on the order of $0.3 M_{\odot} \text{ yr}^{-1}$.

Again, despite the evidence of ongoing star formation and an abundance of H I emission, we do not detect any significant CO emission in this region. Our 7-point mosaic covered all the H I emission (Williams, Yun, & Verdes-Montenegro 2002) and star formation regions detected by GALEX (Xu et al. 2005) and reached a sensitivity of 39 mJy bm^{-1} . We discuss the mass detections limits in the next section.

4. Fluxes and Mass Estimates

4.1. Region B

We detect three emission regions within the BIMA primary beam around the tidal tail in HCG 92. The flux for each individual clump in region B is shown in Table 2. The main CO peak on the tidal tail has also been recently detected by Lisenfeld et al. (2004) using the IRAM interferometer. They detect a flux of $4.4 \pm 1.0 \text{ Jy km s}^{-1}$ for this region, which agrees with our value of $3.8 \pm 0.4 \text{ Jy km s}^{-1}$. The IRAM 30-m detects 5.2 Jy km s^{-1} (Lisenfeld et al. 2002, assuming a Jy-K conversion factor of 4.7). Thus, the flux we detect with BIMA is approximately 70% of the single dish flux, suggesting that 30% of the molecular gas structures are on scales larger than approximately $8''$.

Lisenfeld et al. (2004) also detect weak emission at the tip of the tidal tail, which is too faint to be detected in our data. Additionally, the IRAM 30-m maps to not extend far enough to cover the two weaker emission peaks in the tidal tail region (SQB NW and SQB SE), so we cannot determine what spatial scales dominate the molecular gas distribution.

To calculate the mass for each clump, we summed the flux over a box that covered the emitting regions. The size of the boxes used is given in column 4 of Table 2. The mass is calculated using the equation

$$M_{\text{mol}}(M_{\odot}) = 1.61 \times 10^4 \left(\frac{\alpha}{\alpha_{\text{Gal}}} \right) d_{\text{Mpc}}^2 S_{\text{CO}} \quad (1)$$

where $\alpha/\alpha_{\text{Gal}}$ is the CO-to-H₂ conversion factor relative to the Galactic value ($\alpha_{\text{Gal}} = 3 \pm$

$1 \times 10^{20} \text{ cm}^{-2}(\text{K km s}^{-1})^{-1}$; Scoville & Sanders (1987)), d_{Mpc} is the distance to Stephan's Quintet in Mpc, and S_{CO} is the $^{12}\text{CO } J=1-0$ flux in Jy km s^{-1} . A factor of 1.36 is included to account for the presence of helium.

Assuming a distance of 88 Mpc (for $H_0 = 75 \text{ km s}^{-1}/\text{Mpc}$) we obtain a molecular mass for the central CO peak of $4.7 \times 10^8 M_{\odot}$ assuming a Galactic CO-to- H_2 conversion factor. If the molecular gas in SQB is similar in its properties to the giant molecular clouds in the Milky Way then we can assume that most of the mass is in clouds $\sim 10^6 M_{\odot}$. In this case, SQB likely consists of $\sim 10^2$ clouds of that mass, which are the precursors to the formation of OB associations. In fact, the $\text{H}\alpha$ imaging of HCG 92 by Iglesias-Paramo & Vilchez (2001) shows that the location of SQB is the only spot in the tidal arm with any $\text{H}\alpha$ emission.

4.2. Regions A, C, and N

We did not detect any CO emission in our observations of either region A, C, or N. In region A our observations reached a noise level of 21 mJy bm^{-1} , while in Region C we reached a noise level of 25 mJy bm^{-1} . Assuming a minimal real detection would be spatially unresolved, with velocity width equal to three continuous velocity channels, we would be unable to detect features more massive than $3.9 \times 10^7 M_{\odot}$ in Region A, and $4.6 \times 10^7 M_{\odot}$ in Region C.

The r.m.s noise reached in the Arc-N region was higher because the sensitivity was spread over 7 fields instead of concentrating on a single field as we did in the other regions. The final maps cover an effective area of $180''$ and reach an r.m.s. of 39 mJy bm^{-1} . At a distance of 88 Mpc, this corresponds to an upper mass of $7.3 \times 10^7 M_{\odot}$.

At these mass limits, we can rule out supergiant molecular clouds such as those observed in the Antennae (Wilson et al. 2003) as the source of the star formation since the supergiant clouds generally have masses of a $10^8 M_{\odot}$. It thus seems most likely that regular giant molecular clouds are the source of the ongoing star formation observed in these three regions.

As discussed in §3.1 our lack of detections in region SQA despite the strong flux detected in this region with the IRAM 30m (Lisenfeld et al. 2002) suggests that the molecular gas in SQA is either diffuse or exists in more than two clumps separated by more than 3.4 kpc.

5. Discussion

5.1. Are these Clouds Self Gravitating?

To determine if this object is gravitationally bound, we can compare the mass determined by the flux with what we would expect from the linewidth if the object is in virial equilibrium. If the object is virialized, then its mass can be determined from the following equation:

$$M_{\text{vir}}(M_{\odot}) = 99 V_{\text{FWHM}}^2 D_{\text{pc}} \quad (2)$$

where V_{FWHM} is the full width half-maximum of the spectral line, and D is the cloud diameter (given by $0.7(D_{\alpha} + D_{\delta})$, where D_{α} and D_{δ} are the molecular clouds diameters along the east-west and north-south directions respectively in parsecs; see Wilson (1995)) and a cloud with a density profile that varies as $r^{3/2}$. Assuming a marginally resolved cloud in our map, we obtain a diameter of 4800 pc. A Gaussian fit to the line profile gives a FWHM of 20.3 km s⁻¹, yielding a virial mass of $2.0 \times 10^8 M_{\odot}$. For the other two clouds, we assume the same diameter (unresolved) but adopt the FWHM line widths given in Table 2 to calculate the virial mass. The results are shown in the last column of Table 2.

Since the molecular mass of SQB determined from the CO flux is greater than the mass derived from the linewidth for a virialized cloud, it is likely that this object is massive enough to be self-gravitating. Thus, this object likely represents a long-lived clump that will survive (given its current star formation rate of 0.3 - 0.5 $M_{\odot}\text{year}^{-1}$ Xu et al. 2005; Lisenfeld et al. 2004) should survive for at least a few $\times 10^8$ years.

One complication to this simple picture has been raised by Hibbard & Barnes (2004) who argue that the kinematics observed in TDGs may not necessarily arise from the gravitational potential of the TDGs, but rather from the flow of gas along tidal arms as a result of the galaxy-galaxy interactions. In this view, the dense concentrations of gas seen in TDGs may be a chance alignment of our line of sight *along* a segment of a tidal arm, yielding a large column density of gas, but without a large volume density. Although these authors cast doubt on the reality of many TDGs, they concede that such objects are expected to form in tidal arms. Hibbard & Barnes (2004) argue that best possible situation in which to determine the dynamical mass (and hence reality) of a TDG is when the viewing geometry is face-on to the tidal arms.

In the case of Stephan’s Quintet, the geometry is difficult to determine. Comparing with previously published interaction models, Sulentic et al. (2001) suggest that the specific interaction that created the more prominent, younger tidal tail coming from NGC 7319 was a low velocity one, with a low inclination with respect to the the disk of NGC 7319. Unfortunately, the disk of NGC 7319 is gas poor and no kinematic estimates of its inclination

are available in the literature. The visible appearance of NGC 7319 and its tidal arm suggest that both lie close to the plane of the sky – nearly face on. Our estimates of the dynamical masses are likely at the lowest possible risk for being affected by poor viewing geometry.

The strong CO flux suggests that the molecular gas in this cloud is optically thin (which is supported by the high $^{12}\text{CO}/^{13}\text{CO}$ ratio reported by Lisenfeld et al. (2004)). At first glance this is not surprising – the first gas to be stripped off during an encounter should be the outer gas, which in spiral galaxies is most often at lower metallicities. However, spectroscopy by Lisenfeld et al. (2004) has shown the oxygen abundance ($12 + \log \text{O}/\text{H}$) to be 8.7, nearly equal to the solar value. This is high for the outer regions of typical spiral galaxies, and is high for other TDGs (Duc et al. 2004). Since HCG 92 is believed by many authors to have been the site of repeated encounters, it is possible that by the time the “Young Tail” was formed all the gas from the outer regions had already been stripped away. The gas we observe in SQB may therefore be from the interior of NGC 7319.

The two clouds candidates identified in the “Old Tail”, OT1 and OT2, if real, are more likely to be from the outer regions of their parent galaxy.

If the gas is optically thin, but a low metal abundance is not the reason, it is likely this state is caused by the influence on the ISM of the prominent star forming region in SQB. This idea was proposed by Lisenfeld et al. (2004) to explain the high $^{12}\text{CO} / ^{13}\text{CO}$ ratio they observed. It is consistent with recent estimates of the star formation rate, which range from $0.5 \text{ M}_{\odot}\text{yr}^{-1}$ (Lisenfeld et al. 2004) to $0.3 \text{ M}_{\odot}\text{yr}^{-1}$ (Xu et al. 2005).

For some nearby starburst galaxies it has been argued that the low opacity of the CO emission could cause a reduction in the CO-to- H_2 conversion factor ($\alpha/\alpha_{\text{Gal}}$) (e.g. Harrison, Henkel & Russell (1999) among others). If true this means we are overestimating the molecular mass. This would lead to our molecular mass being an upper limit, and would make our arguments about the gravitationally bound nature of SQB weaker.

5.2. CO- H_2 Conversion Factor Limits

Adopting the method used by Wilson (1995) we can estimate the CO-to- H_2 conversion factor ($\alpha/\alpha_{\text{Gal}}$) by assuming the clouds are virialized, then seeing what value of $\alpha/\alpha_{\text{Gal}}$ is needed to equate the virial mass to the molecular mass. Since the clouds in this study are not resolved, we will only be able to place constraints on $\alpha/\alpha_{\text{Gal}}$.

For unresolved clouds, our virial mass will be an over-estimated. Our molecular mass will also likely be an overestimate, but to a lesser degree. To calculate $\alpha/\alpha_{\text{Gal}}$, we set equation

number (1) equal to equation number (2) and solve for $\alpha/\alpha_{\text{Gal}}$. More simply put, $\alpha/\alpha_{\text{Gal}} = M_{\text{vir}}/M_{\text{mol,Gal}}$ where $M_{\text{mol,Gal}}$ is the molecular mass determined assuming a Galactic value for $\alpha/\alpha_{\text{Gal}}$. This yields values of $\alpha/\alpha_{\text{Gal}}$ of 0.4, < 0.4 and < 1 for the clouds SQB, SQB SE and SQB NW, respectively. Despite the near solar metal abundance, there is at least some evidence for a non-Galactic value of $\alpha/\alpha_{\text{Gal}}$ in CO emission in the tidal arms of HCG 92.

6. Summary

We present the first complete high resolution study of molecular gas in Stephan’s Quintet. Our observations are centered on all major overlap regions in this interacting system in order to study the Tidal Dwarf Galaxy population and the conditions resulting in the intracluster star formation activity observed at other wavelengths.

The wide field of view of the BIMA array enable to detect 7 separate clumps of molecular gas in the new and old tidal tails to the east of Stephan’s Quintet. One of these clumps has already been studied with the Plateau de Bure interferometer by Lisenfeld et al. (2004) but the remaining 6 clumps are new detections. Of these 6, two are well within the primary beam, and likely correspond with the bright “New” tidal tail to the east of Stephan’s Quintet. The remaining four detections are tentative detections at or just beyond the primary beam and lie coincident (spatially and in velocity) with the “Old Tail” region of Stephan’s Quintet.

All but one of the CO clumps associated with the new and old tails correspond well with the velocity of and distribution of the H I observation of Williams, Yun, & Verdes-Montenegro (2002). They also correspond well spatially with the evidence of on-going star formation discovered by recent GALEX observations (Xu et al. 2005). One of the clumps in the new tail (SQB NW) however does not seem to have any corresponding H I emission, but there is evidence of star formation seen in UV images of this region. The nature of this region is a bit of a mystery and will need to be studied further at other wavelengths.

Adopting a Galactic CO-to-H₂ conversion factor, we estimate the molecular masses for these clumps to be on the order of $1 - 5 \times 10^8 M_{\odot}$. The linewidths for these regions suggests virial masses of approximately 50% of the molecular mass, suggesting that these clouds are gravitationally bound, non-transient objects. Our data shows some evidence that the Galactic value of the CO-to-H₂ conversion factor is not appropriate in this near solar metallicity region.

In all other regions we did not detect any significant CO emission. This is somewhat surprising since the IRAM 30-m observations by Lisenfeld et al. (2002) showed strong CO

emission in the intracluster starburst region (SQ A). Our observation of SQ A reached a sensitivity of 21 mJy bm^{-1} (at 5 km s^{-1} velocity resolution) corresponding to a mass sensitivity of $3.9 \times 10^7 M_{\odot}$ (for an unresolved source). Our lack of detection suggests the molecular ISM in this starburst either consists of a diffuse gas or at least 3 clumps separated by over 3 kpc.

G. R. P. is supported in part by NSF grant AST-0228974 and by the State of Maryland via support of the Laboratory for Millimeter-Wave Astronomy. We thank the referee for the careful comments that greatly improved the quality of this paper. The authors are grateful to Lourdes Verdes-Montenegro for providing the H I data cube of HCG 92. We also thank Nathaniel Taylor for waiting until this paper was submitted, allowing an extra week of Chris' attention, and Melissa for her patience.

REFERENCES

- Alves, J., Lada, C. J., & Lada, E. A. 1999, *ApJ*, 515, 265
- Braine, J., Duc, P.-A., Lisenfeld, U., Charmandaris, V., Vallejo, O., Leon, S. & Brinks, E. 2001, *A&A*, 378, 51
- Charlton, J. C., Gallagher, S. C., & Palma, C. 2004, *S&T*, 108, 30
- Duc, P.-A., Brinks, E., Wink, J. & Mirabel, I. 1997, *A&A*, 326, 537
- Duc, P.-A., Brinks, E., Springel, V., Pichardo, B., Weilbacher, P. & Mirabel, I.F. 2001, *AJ*, 120, 1238
- Duc, P.-A., Bournaud, F. & Masset, F., 2004, in *IAU Symposium 217, Recycling Intergalactic and Interstellar Matter*, eds. Duc, P.-A., Braine, J. & Brinks, E., *Astronomical Society of the Pacific*, 550
- Duc, P.-A. & Mirabel, I.F. 1994, *A&A*, 289, 83
- Gallagher, S. C., Charlton, J. C., Hunsberger, S. D., Zaritsky, D., & Whitmore, B. C. 2001, *AJ*, 122, 163
- Gao, Y. & Xu, C. 2000, *ApJL*, 542, L83
- Harrison, A., Henkel, C. & Russell, A. 1999, *MNRAS*, 303, 157

- Helfer, T. T., Thornley, M. D., Regan, M. W., Wong, T., Sheth, K., Vogel, S. N., Blitz, L., & Bock, D. C.-J. 2003, *ApJS*, 145, 259
- Hibbard, J.E. & Barnes, J.E. 2004, in *IAU Symposium 217, Recycling Intergalactic and Interstellar Matter*, eds. Duc, P.-A., Braine, J. & Brinks, E., *Astronomical Society of the Pacific*, 510
- Iglesias-Paramo, J., & Vilchez, J. M., 2001, *ApJ*, 550, 204
- Lisenfeld, U. Braine, J., Duc, P.-A., Leon, S. Charmandaris, V. & Brinks, E. 2002, *A&A*, 394, 823
- Lisenfeld, U. Braine, J., Duc, P.-A., Brinks, S. Charmandaris, V. & Leon, S., 2004, *astro-ph/0407473*
- Mendes de Oliveira, C., Plana, H., Armam, P., Balkowski, C. & Bolte, M. 2001, *AJ*, 121, 2524
- Mirabel, I.F., Lutz, D. & Maza, J. 1991, *A&A*, 243, 367
- Sault, R. J., Teuben, P. J., & Wright, M. C. H. 1995, *ASP Conf. Ser. 77: Astronomical Data Analysis Software and Systems IV*, 4, 433
- Schweizer, F. 1978, *Structure and Properties of Nearby Galaxies*, ed. E.M. Burkhuysen & R. Wielebinski, p. 279
- Scoville, N. Z., & Sanders, D. B. 1987, *ASSL Vol. 134: Interstellar Processes*, 21
- Sulentic, J.W., Rosado, M., Dultzin-Hacyan, D., Verdes-Montenegro, L., Trinchieri, G., Xu, C. & Pietsch, W. 2001, *AJ*, 122, 2993
- Taylor, C.L., Kobulnicky, H.A. & Skillman, E.D. 1998, *AJ*, 116, 2746
- Welch, W. J., et al. 1996, *PASP*, 108, 93
- Williams, B. A., Yun, M. S., & Verdes-Montenegro, L. 2002, *AJ*, 123, 2417
- Wilson, C. D. 1995, *ApJ*, 448, L97
- Wilson, C. D., Scoville, N., Madden, S. C., & Charmandaris, V. 2003, *ApJ*, 599, 1049
- Xu, C., Sulentic, J.W. & Tuffs, R. 1999, *ApJ*, 512, 178
- Xu, C.K., et al., 2005, *ApJ*, 619, L95

Yun, M. S., Verdes-Montenegro, L., del Olmo, A., & Perea, J. 1997, *ApJ*, 475, L21

Zwicky, F. 1956, *Ergebnisse de Exakten Naturwissenschaften* 29, 34

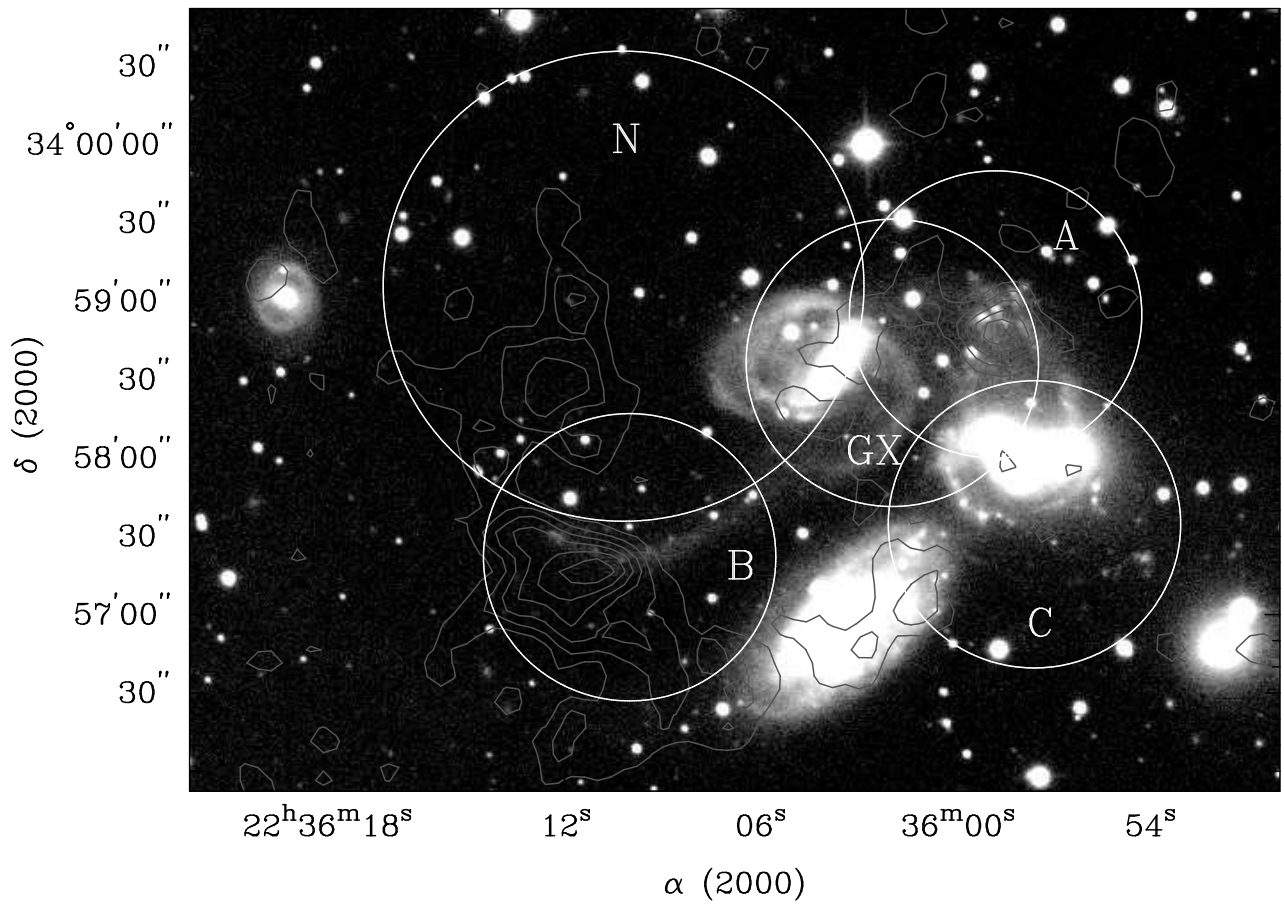


Fig. 1.— The four regions of HCG 92 observed by us with the BIMA array (labeled A, B, C, and N) as well as the region observed by Gao & Xu (2000) (labeled GX). The underlying image is an NOAO photograph taken by N.A.Sharp/NOAO/AURA/NSF. The gray contours are the HI data from Williams, Yun, & Verdes-Montenegro (2002).

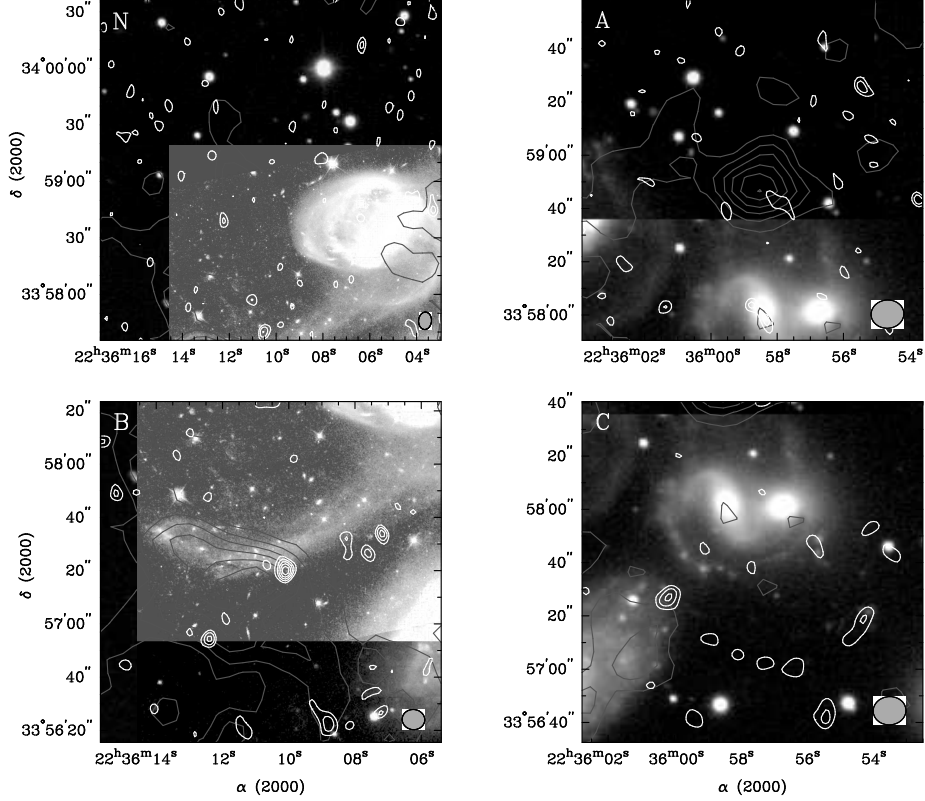


Fig. 2.— A raw moment zero map for the four regions observed in this study. No clipping or masking has been applied in order to show the noise levels reached in the regions where there are no detections. The contour levels are 2,3,4... times the r.m.s. noise in the moment map. For the three regions without a CO detection, we integrate over 200 km s⁻¹ around the H I peak. For Region N, the r.m.s. is 1.41 Jy bm⁻¹ km s⁻¹ from 6500-6700 km s⁻¹; for Region A the noise is 1.04 Jy bm⁻¹ km s⁻¹ from 5900-6100 km s⁻¹; for Region B the noise is 0.65 Jy bm⁻¹ km s⁻¹ from 6500-6660 km s⁻¹; and for Region C the noise is 0.64 Jy bm⁻¹ km s⁻¹ from 6650-6850 km s⁻¹.

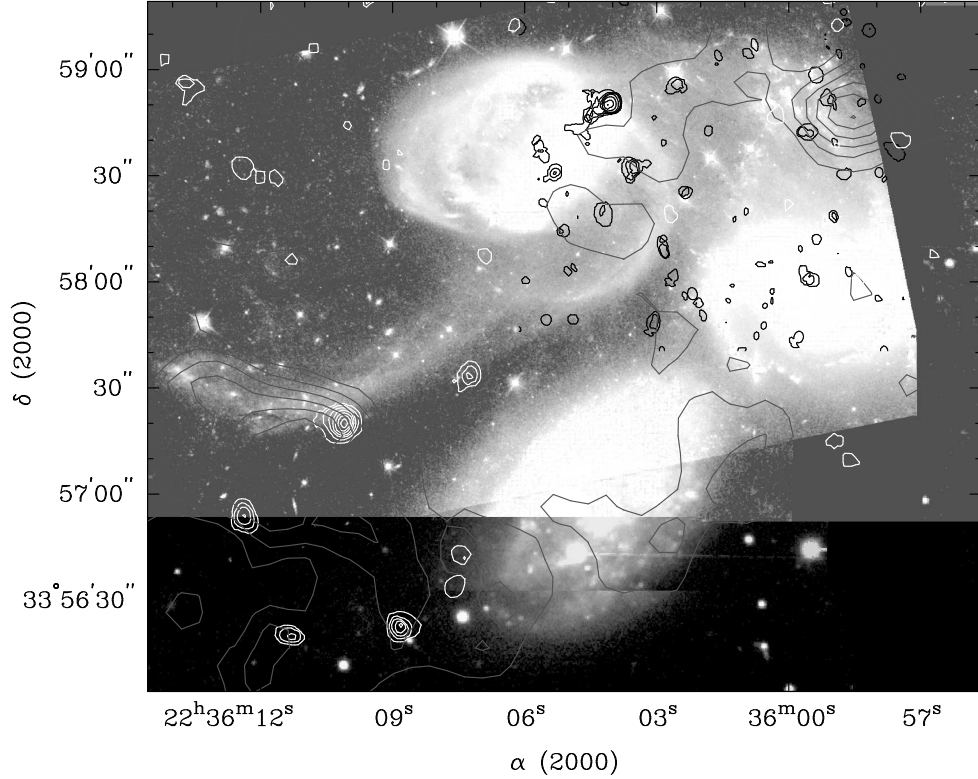


Fig. 3.— $^{12}\text{CO } J=1-0$ contours overlaid on a composite image of HCG 92. The white contours show the data obtained as part of this study. The grey contours are the H I observations of Williams, Yun, & Verdes-Montenegro (2002). The black contours are the CO contours from the Gao & Xu (2000) study. The high resolution greyscale data is from HST observations by Gallagher et al. (2001); the lower resolution data used to fill in the regions not covered by HST are taken from the Arp Catalog of Peculiar Galaxies. The contour levels for all maps are the same in order to allow comparison of CO brightness between the regions with detections. The contour levels are 0.5, 1.0, 1.5 ... $\text{Jy } \text{bm}^{-1} \text{ km s}^{-1}$. The moment-0 CO maps in this figure and Figure 4 used a masking technique that does not show emission with a $\text{SNR} < 2$. Thus, the resulting map shows some features than are not visible in the “raw” map shown in Figure 2.

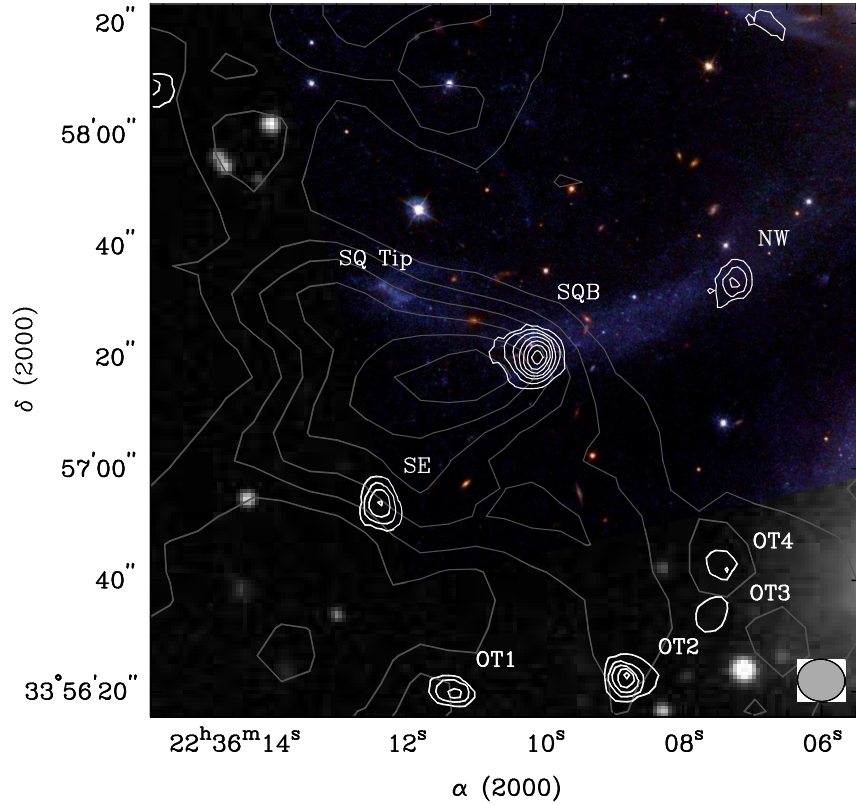


Fig. 4.— A close up look at the CO emission detected in the tidal tail region. The contour levels are 0.5, 1.0, 1.5...3.5 $\text{Jy bm}^{-1} \text{ km s}^{-1}$. The synthesized beam is shown as a black circle in the lower right corner. The primary beam of this field is $100''$, indicating that the regions labeled OT1, OT2, OT3, and OT4 fall just outside of the primary beam. Their spatial correspondence with the “Old Tail” and velocity coincidence with the H I observations of this region provides some evidence in support of the reality of these features.

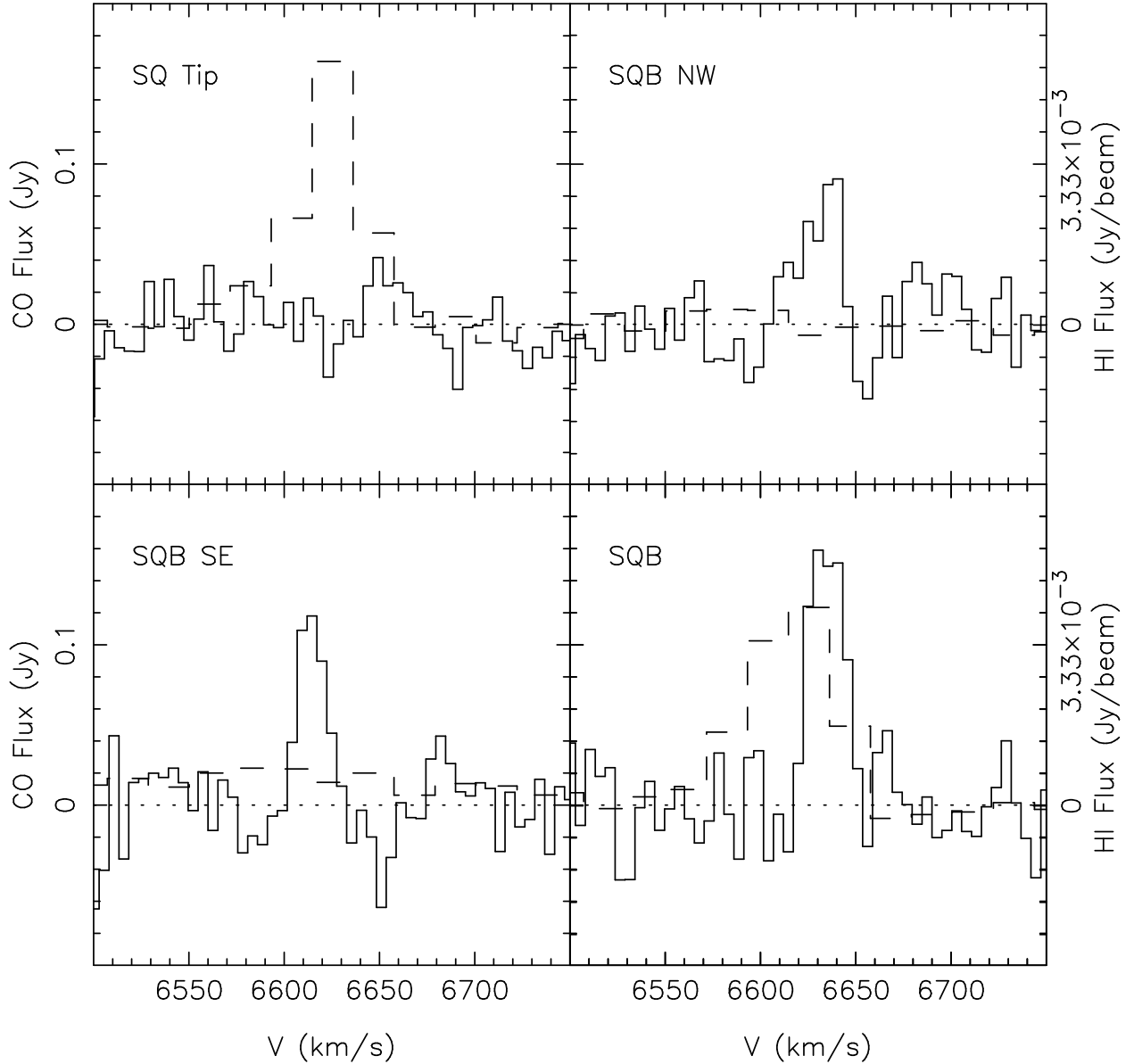


Fig. 5.— Individual $^{12}\text{CO } J=1-0$ and H I spectra for the four regions discussed in the text. The solid line is the CO data from this study, and the dashed line is the H I data from Williams, Yun, & Verdes-Montenegro (2002). The left axis label corresponds to the CO and the right axis labels apply to the H I spectra. The upper left panel is the non-detection of the “SQ Tip” region shown in Lisenfeld et al. (2004); the upper right panel is the weaker emission region to the north-west of the tidal tail in the IGM (SQB NW); the lower left panel is the peak in the south-east of the tidal tail (SQB SE); and the lower right panel is the central emission peak on the tidal tail (SQB). Note, that there *is* significant H I emission in SQB SE, it is just scaled down in order to be able to show the H I emission in region SQB and SQ Tip with the same vertical scale.

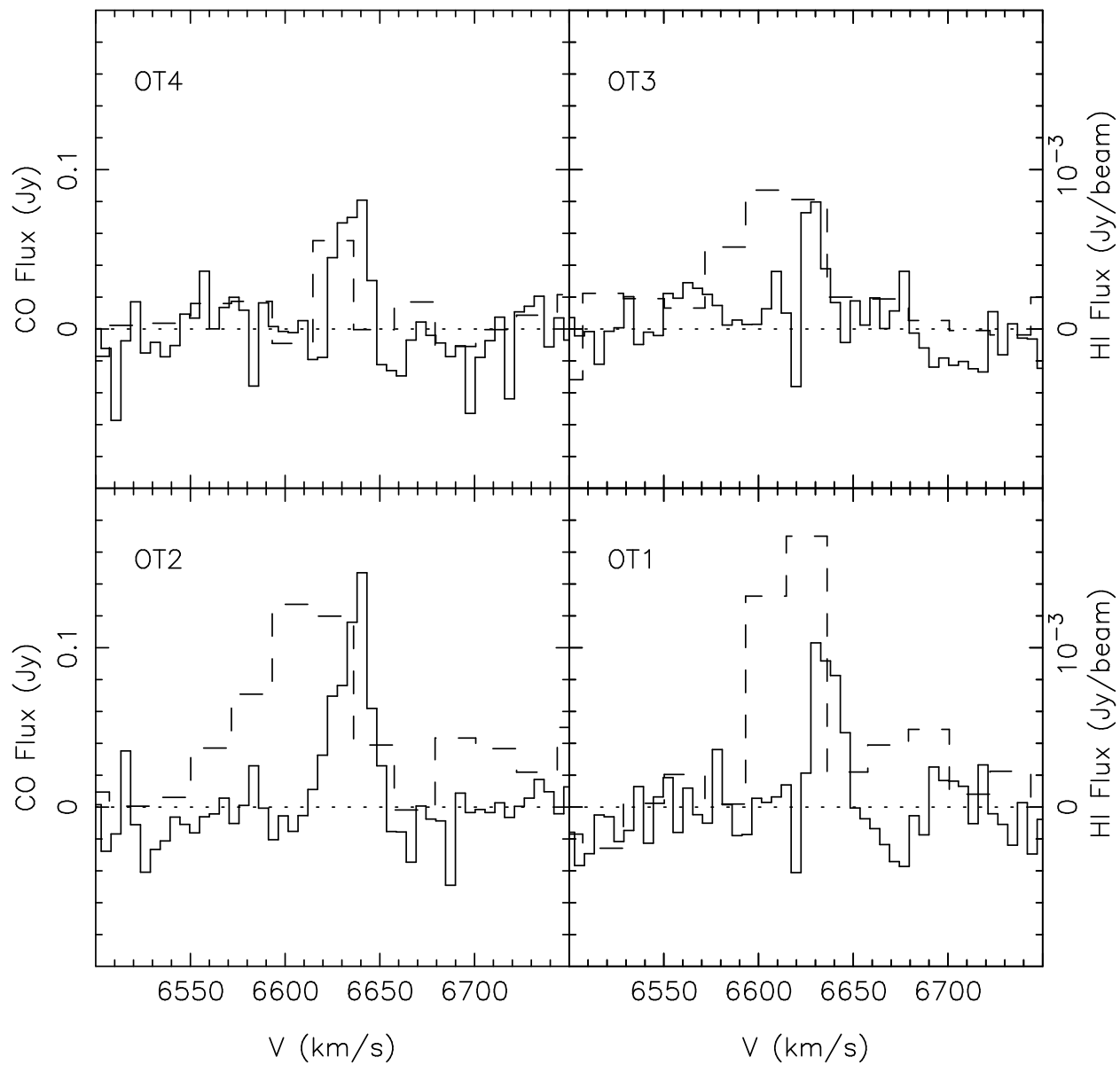


Fig. 6.— Individual $^{12}\text{CO } J=1-0$ spectra for the four emission regions discussed just outside the primary beam in the Old Tail. The solid line is the CO data from this study, and the dashed line is the H I data from Xu, Sulentic, & Tuffs (1999). The left axis label corresponds to the CO and the right axis labels apply to the H I spectra.

Table 1. Observing Parameters

label	RA (J2000)	Dec. (J2000)	V_{LSR} (km s^{-1})	pntgs	f.o.v (")	synth. beam "×"	r.m.s @ 5km s^{-1} (mJy bm^{-1})
SQA	22 ^h 35 ^m 58.7 ^s	33°58'55"	6050	1	100	7.1×6.3	21
SQB	22 ^h 36 ^m 10.5 ^s	33°57'20"	6625	1	100	8.5×7.5	23
SQC	22 ^h 35 ^m 57.6 ^s	33°57'37"	6600	1	100	12.2×10.6	25
Arc-N	22 ^h 36 ^m 12.0 ^s	33°58'28"	6625	7	180	9.3×6.8	39

Table 2. New Tail Line Parameters

label	RA (J2000)	Dec. (J2000)	area ("×")	flux (Jy km s^{-1})	FWHM (km s^{-1})	V (km s^{-1})	M_{gas} (M_{\odot})	M_{vir} (M_{\odot})
SQB	22 ^h 36 ^m 10.1 ^s	33°57'20"	13×11	3.8±0.4	20.3	6635	4.7×10^8	2.0×10^8
SQB SE	22 ^h 36 ^m 12.3 ^s	33°56'53"	6×10	2.2±0.4	16.1	6614	2.7×10^8	$< 1.2 \times 10^8$
SQB NW	22 ^h 36 ^m 07.3 ^s	33°57'34"	8×8	1.9±0.4	22.2	6632	2.4×10^8	$< 2.3 \times 10^8$

Table 3. Old Tail Line Parameters

label	RA (J2000)	Dec. (J2000)	area ("×")	flux (Jy km s^{-1})	FWHM (km s^{-1})	V (km s^{-1})	M_{gas} (M_{\odot})	M_{vir} (M_{\odot})
SQOT 1	22 ^h 36 ^m 11.3 ^s	33°56'20"	14×10	1.8±0.3	15.2	6636	2.2×10^8	$< 1.1 \times 10^8$
SQOT 2	22 ^h 36 ^m 08.8 ^s	33°56'23"	14×12	2.8±0.4	21.0	6636	3.5×10^8	$< 2.1 \times 10^8$
SQOT 3	22 ^h 36 ^m 07.6 ^s	33°56'34"	10×10	0.9±0.3	9.9	6629	1.1×10^8	$< 0.5 \times 10^8$
SQOT 4	22 ^h 36 ^m 07.4 ^s	33°56'43"	8×8	1.4±0.3	16.4	6635	1.7×10^8	$< 1.3 \times 10^8$